Combined Changes in Chloride Regulation and Neuronal Excitability Enable Primary Afferent Depolarization to Elicit Spiking without Compromising its Inhibitory Effects

Petri Takkala[1,2◉], Yi Zhu[3◉], Steven A. Prescott[1,2,3,4]*

1 Neurosciences and Mental Health, The Hospital for Sick Children, Toronto, Ontario, Canada, **2** Institute of Medical Science, University of Toronto, Toronto, Ontario, Canada, **3** Center for Pain Research, Department of Anesthesiology, University of Pittsburgh, Pittsburgh, Pennsylvania, United States of America, **4** Department of Physiology and the Institute of Biomaterials and Biomedical Engineering, University of Toronto, Ontario, Canada

◉ These authors contributed equally to this work.
* steve.prescott@sickkids.ca

Abstract

The central terminals of primary afferent fibers experience depolarization upon activation of $GABA_A$ receptors ($GABA_A R$) because their intracellular chloride concentration is maintained above electrochemical equilibrium. Primary afferent depolarization (PAD) normally mediates inhibition via sodium channel inactivation and shunting but can evoke spikes under certain conditions. Antidromic (centrifugal) conduction of these spikes may contribute to neurogenic inflammation while orthodromic (centripetal) conduction could contribute to pain in the case of nociceptive fibers. PAD-induced spiking is assumed to override presynaptic inhibition. Using computer simulations and dynamic clamp experiments, we sought to identify which biophysical changes are required to enable PAD-induced spiking and whether those changes necessarily compromise PAD-mediated inhibition. According to computational modeling, a depolarizing shift in GABA reversal potential (E_{GABA}) and increased intrinsic excitability (manifest as altered spike initiation properties) were necessary for PAD-induced spiking, whereas increased $GABA_A R$ conductance density ($\bar{g}_{GABA}$) had mixed effects. We tested our predictions experimentally by using dynamic clamp to insert virtual $GABA_A R$ conductances with different E_{GABA} and kinetics into acutely dissociated dorsal root ganglion (DRG) neuron somata. Comparable experiments in central axon terminals are prohibitively difficult but the biophysical requirements for PAD-induced spiking are arguably similar in soma and axon. Neurons from naïve (i.e. uninjured) rats were compared before and after pharmacological manipulation of intrinsic excitability, and against neurons from nerve-injured rats. Experimental data confirmed that, in most neurons, both predicted changes were necessary to yield PAD-induced spiking. Importantly, such changes did not prevent PAD from inhibiting other spiking or from blocking spike propagation. In fact, since the high value of $\bar{g}_{GABA}$ required for PAD-induced spiking still mediates strong inhibition, we conclude that PAD-induced spiking does not represent failure of

presynaptic inhibition. Instead, diminished PAD caused by reduction of $\bar{g}_{GABA}$ poses a greater risk to presynaptic inhibition and the sensory processing that relies upon it.

Author Summary

Postsynaptic $GABA_AR$ mediate inhibition by causing hyperpolarization or by preventing (shunting) the depolarization caused by concurrent excitatory input. Presynaptic $GABA_AR$ work differently, in the spinal cord at least. Because of their higher-than-equilibrium intracellular chloride concentration, the central terminals of primary afferent fibers are depolarized by activation of $GABA_AR$. This so-called primary afferent depolarization, or PAD, nonetheless reduces spike propagation and synaptic release from those fibers because of shunting effects and sodium channel inactivation. But those inhibitory effects can be diminished under certain pathological conditions; in fact, the emergence of dorsal root reflexes suggests that PAD can become paradoxically excitatory. The biophysical basis for this paradoxical excitation has been hinted at by experiments, but here, for the first time, we use computational modeling and dynamic clamp experiments to decipher how distinct contributing factors interact to enable PAD-induced spiking. Our results suggest that PAD-induced spiking requires a shift in GABA reversal potential plus changes in intrinsic excitability that allow for repetitive spiking during sustained depolarization. Inhibitory effects of PAD are retained under conditions in which $GABA_AR$ activation causes transient spiking and are only lost if $GABA_AR$ activation can evoke repetitive spiking.

Introduction

Synaptic inhibition regulates transmission of sensory signals through the spinal cord. Importantly, numerous chronic pain conditions are associated with diminished inhibition [1–5] and pharmacological blockade of inhibition at the spinal level has been shown to reproduce many features of those chronic pain conditions [6–9]. Decreased transmitter release, reduced $GABA_A$/glycine receptor function, and altered chloride regulation are all potential *dis*inhibitory mechanisms, but pre- and postsynaptic inhibition are not equally susceptible to certain pathological changes; for instance, the potassium-chloride co-transporter KCC2 is not expressed in primary afferent neurons, meaning disinhibitory effects of KCC2 downregulation [10] are attributable entirely to reduced postsynaptic inhibition, in cells that express KCC2. KCC3 is expressed in some primary afferents and can extrude chloride under isosmotic conditions [11,12] but it remains unknown whether KCC3 is altered under pathological conditions. Yet selective disruption of presynaptic inhibition can cause mechanical and thermal hypersensitivity [13] and presynaptic expression of the α2 GABA receptor subunit is necessary for the antihyperalgesic effect of diazepam [14]. These observations affirm that presynaptic $GABA_AR$-mediated inhibition also plays a key role in nociception.

Pre- and postsynaptic inhibition in spinal cord are mechanistically distinct. Postsynaptically, in mature spinal neurons, the reversal potential associated with $GABA_AR$ (E_{GABA}) is normally around -70 mV [10], meaning $GABA_AR$ activation reduces depolarization caused by concurrent excitatory input. Presynaptically, in the central terminals of primary afferents, E_{GABA} is normally around -35 mV because chloride is actively loaded into primary afferents by the sodium-potassium-chloride co-transporter NKCC1 [13,15–17], thus $GABA_AR$ activation causes depolarization. Contrary to the presumed excitatory effect of depolarization, primary

afferent depolarization (PAD) mediates inhibitory effects via sodium channel inactivation and shunting [18–21]. However, PAD can sometimes trigger spikes that conduct antidromically, thus producing what is referred to as a dorsal root reflex (DRR) [22]. One theory holds that antidromically conducted spikes mediate an inhibitory effect by colliding with and blocking othrodromically conducted spikes originating in the periphery [23,24]; however, collisions are unlikely since the latency to travel the full length of the nerve is short relative to the interspike interval at realistic spiking rates. PAD-induced spikes are unlikely to trigger synaptic release from the PAD-affected branch because spike amplitude is attenuated, but PAD-induced spikes that manage to propagate to adjacent, PAD-free branches may trigger synaptic release [25]. The experiments required to test these model predictions are prohibitively difficult. The above theory was formulated for large myelinated proprioceptive afferents involved in locomotion; in contrast, within smaller afferents responsible for nociception, the prevailing view is that PAD-induced spikes occur only under pathological conditions and that DRRs contribute to neurogenic inflammation and hypersensitivity [22,26]. Within this context, PAD-induced spiking is thought to represent conversion of PAD from an inhibitory process to an excitatory one [22].

With respect to biophysical mechanisms, PAD-induced spiking requires $GABA_AR$ activation [27] and NKCC1-mediated chloride loading [28]. Enhanced chloride loading and the consequent depolarizing shift in E_{GABA} has been hypothesized to facilitate PAD-induced spiking [29,30]. Nerve injury increases NKCC1 protein levels and PAD [13,31], and although total NKCC1 expression is not altered by inflammation [32,33], NKCC1 membrane trafficking and phosphorylation are affected by painful stimuli [34]. Notably, inflammation causes a depolarizing shift in E_{GABA} [35] and promotes DRRs in C and Aδ fibers [36]. Increased $GABA_AR$ density and reduced low-threshold potassium channel density have also been hypothesized to promote DRRs [35,37] but the full set of requirements for PAD-induced spiking remains unclear. We sought to identify which biophysical changes, alone or together, enable PAD-induced spiking and how such changes impact PAD-mediated inhibition.

Results

Changes in GABA conductance density $\bar{g}_{GABA}$, its associated reversal potential E_{GABA}, and intrinsic excitability have all been implicated in PAD-induced spiking, as outlined above. To account for whether a neuron spikes transiently or repetitively, and whether spike threshold is sensitive to the rate of depolarization, we discuss excitability in terms of spike initiation dynamics [38]. Rather than characterize further how excitability and GABAergic signalling are pathologically altered, we sought to decipher how known pathological alterations contribute to PAD-induced spiking. To this end, we took an approach distinct from previous studies to determine how isolated and combined changes in each factor–$\bar{g}_{GABA}$, E_{GABA}, and excitability– affect PAD-induced spiking. We began with a minimalist conductance-based computer model to generate predictions that we then tested experimentally in acutely dissociated dorsal root ganglion (DRG) neurons using dynamic clamp. Intracellular recording/stimulation in most axons is prohibitively difficult but sustained depolarization of the soma or axon by optogenetic-based photostimulation evokes transient spiking, although photostimulation of peripheral axon terminals can evoke repetitive spiking in some DRG neurons [39]. It remains unclear how central axon terminals respond to sustained depolarization. We assume here that somatic and axonal spike initiation properties are qualitatively similar, but if axons were more excitable (i.e. more prone to repetitive spiking) than somata, they would operate farther to the right along the "excitability" axis described below. We applied virtual GABA conductances rather than assuming the soma and axon have equivalent $GABA_AR$ densities. As a final step, we confirmed our results in a multicompartment axon model.

PAD-induced spiking in a model neuron

Starting with computer simulations, we co-varied E_{GABA} and intrinsic excitability (controlled by β_w; see Methods) while keeping $\bar{g}_{GABA}$ fixed at 2 nS/pF. The light grey and dark grey regions of the resulting 2-D bifurcation diagram (Fig 1A) show the E_{GABA} and β_w combinations that produce transient and repetitive spiking, respectively. Spiking pattern was determined by the response to GABA conductance "steps". To more accurately simulate different forms of synaptic transmission, other conductance waveforms were tested: phasic inhibition via intrasynaptic GABA$_A$R was modeled by a "fast" synaptic waveform (τ_{rise} = 2 ms; τ_{decay} = 20 ms; see Eq 6); tonic inhibition corresponds to the sustained component of the conductance step, but we also tested a "slow" synaptic waveform with intermediate kinetics to simulate spilled-over GABA asynchronously activating extrasynaptic GABA$_A$R (τ_{rise} = 20 ms; τ_{decay} = 200 ms). Fig 1B shows responses to each stimulus waveform for parameter combinations labeled a-f on Fig 1A. Under control conditions used in the experiments described in this study (E_{GABA} = -35 mV
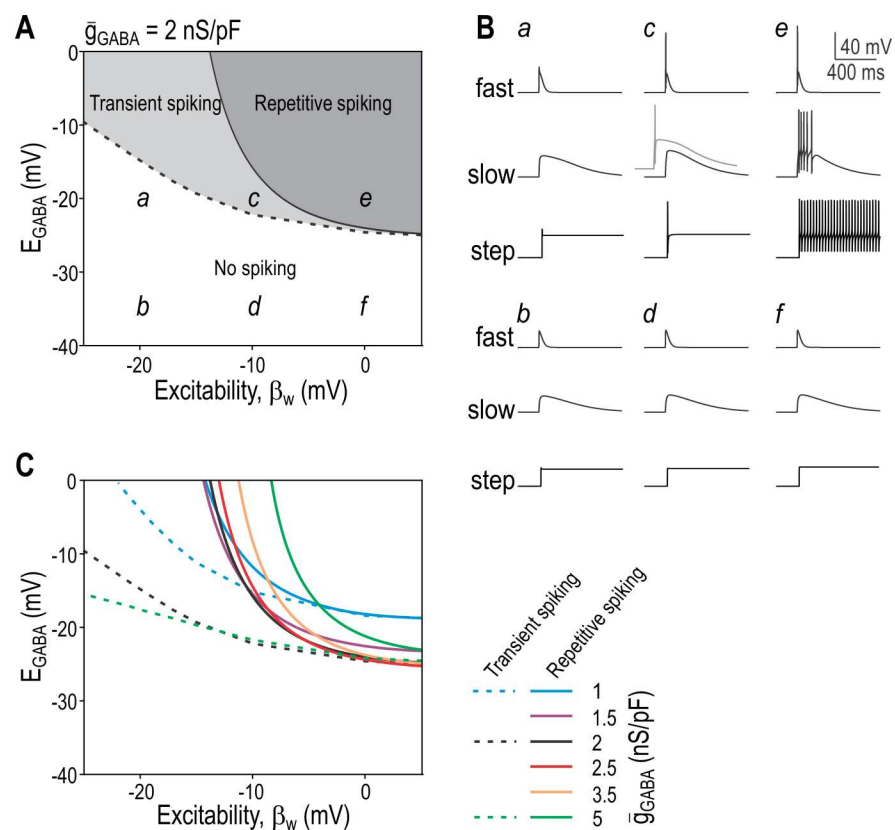

Fig 1. PAD-induced spiking in a neuron model. (A) 2-D bifurcation diagram showing the combinations of E_{GABA} and β_w that allow a GABA conductance step ($\bar{g}_{GABA}$ = 2 nS/pF) to elicit repetitive or transient spiking (dark and light grey regions, respectively). Labels a-f indicate parameter combinations for which sample responses are shown in B. Normal conditions correspond to E_{GABA} = -35 mV and β_w = -20 mV (point b). (B) Sample responses to a *fast* synaptic waveform (τ_{rise} = 2 ms, τ_{decay} = 20 ms), a *slow* synaptic waveform (τ_{rise} = 20 ms, τ_{decay} = 200 ms) and a conductance *step* for parameter combinations labeled in A. Slow-onset conductance requires stronger $\bar{g}_{GABA}$ (3.5 nS/pF, grey trace in c) to elicit transient spiking than a fast-onset conductance; all black traces are for $\bar{g}_{GABA}$ = 2 nS/pF. (C) 2-D bifurcation analysis described in A was repeated for different $\bar{g}_{GABA}$ values. Dashed and solid lines show borders for the transient and repetitive spiking regions, respectively. Increasing $\bar{g}_{GABA}$ from 1 to 2 nS/pF (cyan → black) caused a downward shift in both borders but further increases (black → green) caused little change in the former and a rightward shift in the latter, indicating that increased $\bar{g}_{GABA}$ confers increased spiking only to a certain point, beyond which further increase actually reduces spiking.

doi:10.1371/journal.pcbi.1005215.g001

and β_w = -20 mV; point *b*), GABA conductance caused depolarization but no spiking. PAD-induced repetitive spiking required a combined depolarizing shift in E_{GABA} and β_w (point *e*) whereas transient spiking required a smaller increase in β_w (point *c*) and could result solely from a large change in E_{GABA}. By comparison, an isolated change in β_w could not enable PAD-induced spiking. As illustrated in panel *c* of Fig 1B, slow-onset GABA$_A$R input required stronger input to elicit spiking because transient spiking involves a spike initiation mechanism that is sensitive to the rate of depolarization [40].

Next, we repeated the 2-D bifurcation analysis for different $\bar{g}_{GABA}$ values to produce a family of curves (**Fig 1C**). The dashed curve demarcating the minimum requirements for transient spiking shifted downward as $\bar{g}_{GABA}$ was increased. The solid curve demarcating the minimum requirements for repetitive spiking also shifted downward for an initial increase in $\bar{g}_{GABA}$ but shifted rightward as $\bar{g}_{GABA}$ was increased further, indicating that GABA$_A$R activation is maximally excitatory at intermediate densities. Somatic recordings have demonstrated somatic $\bar{g}_{GABA}$ between 0.2 and 0.5 nS/pF [35] and the absolute $\bar{g}_{GABA}$ values reported by Chen et al. [13] correspond to approximately 0.1 nS/pF after conversion to densities based on estimated surface areas. Axonal $\bar{g}_{GABA}$ may differ from somatic $\bar{g}_{GABA}$ (given precedents for differential ion channel distribution [41]) but measuring $\bar{g}_{GABA}$ in central axon terminals is prohibitively difficult. Our experimental approach does not rely on measuring axonal $\bar{g}_{GABA}$ but, instead, was designed to determine the minimum $\bar{g}_{GABA}$ required (for different E_{GABA} and intrinsic neuronal excitability) to enable PAD-induced spiking; comparing this value against measured $\bar{g}_{GABA}$ (in the soma) reveals whether the density of native GABA receptors is sufficient to evoke spiking under different conditions. It remains unclear what $\bar{g}_{GABA}$ would be necessary to evoke spiking in central axon terminals.

PAD-induced transient spiking in DRG neurons

To test the simulation predictions described above, we conducted experiments in acutely dissociated DRG somata using an approach distinct from previous studies. Rather than activating native GABA$_A$Rs by puffing GABA (which would produce a current whose conductance, reversal potential and kinetics are not easily measured or independently manipulated), we used dynamic clamp to apply a virtual conductance whose parameters are precisely and independently controllable. In this way, we quantified the minimum *virtual* $\bar{g}_{GABA}$ required to elicit spiking under different conditions. Importantly, because virtual $\bar{g}_{GABA}$ can be higher than native $\bar{g}_{GABA}$, the density of native GABA$_A$R does not limit our studies; indeed, failure of GABA puffs to evoke spikes in previous studies [13,35,42] suggests that somatic $\bar{g}_{GABA}$ is normally too low to produce spikes, but $\bar{g}_{GABA}$ may be higher in central axon terminals. In dynamic clamp, the voltage recorded from a neuron is passed to a computer, which, in real time, uses voltage to calculate current that is injected back into the patched neuron, thereby introducing a virtual conductance [43]. This approach allows manipulations to be applied like in computer simulations but to real neurons, such that we can avoid modeling the neuron (and making any assumptions about intrinsic excitability) and test directly how *virtual* GABA$_A$R input affects *native* voltage-gated channels controlling spike initiation. Notably, photostimulation-based testing of axonal excitability has revealed transient spiking comparable to that observed in somata [39] but the excitability of central axon terminals remains uncertain. If central axon terminal and somatic excitability are similar, then the requirements for PAD-induced spiking ascertained for the soma can be extrapolated to those terminals; on the other hand, if those terminals are more excitable, they would operate farther to the right on the excitability axis depicted in the inset of **Fig 2A**.

To begin, we tested virtual GABA conductances in neurons from naïve animals before and after reproducing the hyperexcitability associated with nerve injury by blocking K$_v$1-type potassium channels with 4-AP [44,45]; this corresponds in the model to setting β_w to less
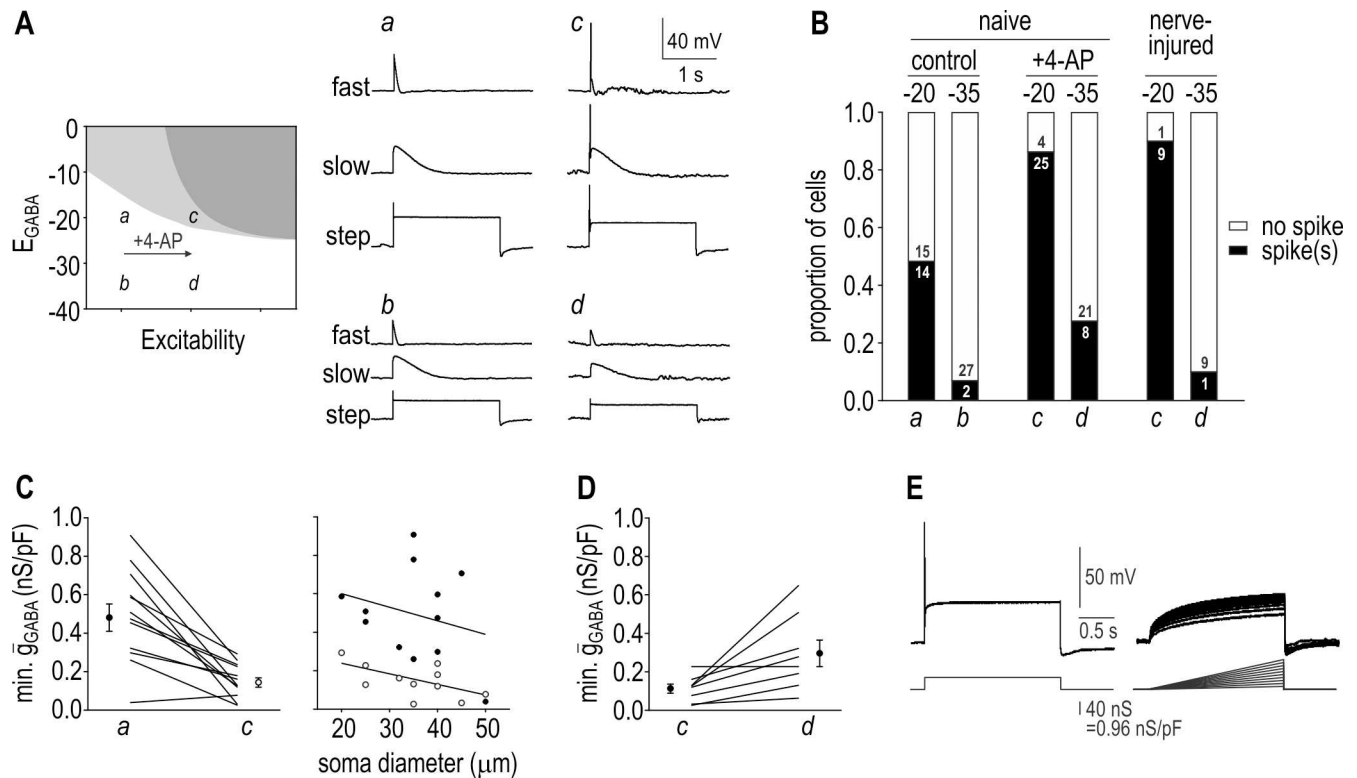
Fig 2. PAD-induced transient spiking in DRG neurons. (A) Sample responses to virtual GABA conductance applied via dynamic clamp. Labels *a-d* on cartoon indicate testing conditions and are referred to in all subsequent panels. Most neurons, like the typical one illustrated here, spiked only for E_{GABA} = -20 mV and after being made hyperexcitable by exposure to 2.5 mM 4-AP (point *c*). **(B)** Summary of the proportion of neurons responding with or without spikes to virtual PAD. Numbers inside each bar indicate the number of cells. A total of 29 neurons from naïve rats were tested before and after 4-AP and for each E_{GABA}. A total of 10 neurons from nerve-injured rats were tested for each E_{GABA}. The proportion of spiking/non-spiking cells was compared between conditions using Fisher's exact tests (see Results). **(C)** Left panel summarizes the minimum $\bar{g}_{GABA}$ required to elicit spiking in cells that spiked both before and after 4-AP for E_{GABA} = -20 mV. Minimum $\bar{g}_{GABA}$ was significantly reduced from 0.76 ± 0.19 to 0.20 ± 0.05 nS/pF (mean ± SEM) by 4-AP (p = 0.005, two-way repeated measures ANOVA and Tukey test). These values are lower than observed in simulations in Fig 1; therefore, we adjusted the neuron model to reproduce this higher sensitivity to $\bar{g}_{GABA}$. As illustrated in S1 Fig, this revised model shows the same relationship between E_{GABA} and excitability (β_w) as seen in Fig 1. Right panel shows minimum $\bar{g}_{GABA}$ plotted against soma diameter. Soma diameter, which correlates with fiber type, did not significantly affect minimum $\bar{g}_{GABA}$ or the effect of 4-AP (p = 0.61 and 0.29, respectively; two-way repeated measures ANOVA). **(D)** Summary of the minimum $\bar{g}_{GABA}$ required to elicit spiking in cells that spiked for each E_{GABA} value after 4-AP. The depolarizing shift in E_{GABA} from -35 mV to -20 mV caused a significant reduction (p<0.022, paired *t*-test) from 0.30 ± 0.07 nS/pF to 0.11 ± 0.02 nS/pF. **(E)** Sample responses from a typical neuron tested with g_{GABA} steps and ramps. The minimum $\bar{g}_{GABA}$ required to elicit transient spiking when applied as a step was 40 nS (or 0.96 nS/pF after normalization by membrane capacitance) but a ramp with 2.5x greater peak amplitude failed to elicit spiking. E_{GABA} = -20 mV.

doi:10.1371/journal.pcbi.1005215.g002

negative values. Testing with different E_{GABA} and stimulus waveforms, we systematically increased $\bar{g}_{GABA}$ to try to elicit spiking. As illustrated for a typical cell in **Fig 2A**, PAD was most likely to produce spiking after application of 4-AP *and* a depolarizing shift in E_{GABA} to -20 mV. **Fig 2B** summarizes the proportion of cells in which PAD-induced spiking was observed under each test condition. For cells from naïve animals tested with E_{GABA} = -35 mV, 4-AP increased the proportion exhibiting PAD-induced spiking but not significantly (p = 0.079; Fisher's exact test) whereas the 4-AP effect was highly significant for E_{GABA} = -20 mV (p = 0.004). Shifting E_{GABA} from -35 mV to -20 mV significantly increased the proportion of cells exhibiting PAD-induced spiking both before and after 4-AP ($p < 10^{-3}$ and 10^{-4}, respectively), consistent with the NKCC1 hypothesis of DRR generation [29,30]. But as predicted by our simulations, the proportion of cells with PAD-induced spiking was most significantly increased by the combination of 4-AP and a depolarizing shift in E_{GABA} ($p < 10^{-9}$). Within this data set, two cells were subsequently identified as outliers based on analysis of the

minimum $\bar{g}_{\text{GABA}}$ needed for PAD-induced spiking (see below); removing those outliers did not substantively alter the statistical results reported above.

Based on cells that exhibited PAD-induced spiking before and after 4-AP for E_{GABA} = -20 mV, the minimum $\bar{g}_{\text{GABA}}$ needed to elicit spiking was significantly reduced from 0.49 ± 0.07 nS/pF (mean±SEM) to 0.16 ± 0.03 nS/pF by 4-AP (p = 0.005, Tukey test following ANOVA described below) (**Fig 2C left**). Plotting the same data against soma diameter revealed a trend towards higher minimum $\bar{g}_{\text{GABA}}$ for smaller cells, but soma diameter did not have a significant effect (p = 0.61) and nor did it interact significantly with the 4-AP effect (p = 0.29; two-way repeated measures ANOVA) (**Fig 2C right**). Notably, we report all conductances as densities to correct for the direct effect of membrane surface area on our measurements; however, soma diameter is known to correlate with fiber type [46], and so the insignificant effect of cell size (after normalization by surface area) argues that minimum $\bar{g}_{\text{GABA}}$ does not differ significantly between myelinated (A) and unmyelinated (C) neurons. Of the cells that exhibited PAD-induced spiking for both E_{GABA} values after 4-AP, the minimum $\bar{g}_{\text{GABA}}$ needed to elicit spiking was significantly reduced from 0.30 ± 0.07 nS/pF to 0.11 ± 0.02 nS/pF by shifting E_{GABA} from -35 mV to -20 mV (p = 0.022, paired t-test) (**Fig 2D**). Of the 10 cells tested with both fast and slow g_{GABA} waveforms at E_{GABA} = -20 mV after 4-AP, 7 responded to both stimuli with transient spiking and 2 responded with repetitive spiking. Among transient spiking cells, the slow waveform required higher $\bar{g}_{\text{GABA}}$ than the fast waveform to elicit transient spiking (0.46 ± 0.09 nS/pF vs 0.27 ± 0.09 nS/pF) which, although not a statistically significant difference (p = 0.25; paired t-test), is consistent with a spike initiation mechanism sensitive to the rate of depolarization. By comparison, the two repetitive spiking cells required exactly the same minimum $\bar{g}_{\text{GABA}}$ for the fast and slow waveforms, consistent with a spike initiation mechanism sensitive only to the amplitude of depolarization [40]. Comparing the responses to g_{GABA} steps and ramps illustrates that the latter are far less effective in eliciting transient spiking (**Fig 2E**). All of these experimental data are consistent with simulation results in Fig 1 and S1 Fig.

Like 4-AP, nerve injury increased the proportion of cells exhibiting PAD-induced spiking (bars on right side of **Fig 2B**). Compared against naïve cells without 4-AP, nerve injury caused no change in the proportion of cells exhibiting PAD-induced spiking for E_{GABA} = -35 mV (p = 1) whereas it did significantly increase that proportion for E_{GABA} = -20 mV (p = 0.028; Fisher's exact tests). Nerve injury and treatment of naïve cells with 4-AP resulted in a similar proportion of cells with PAD-induced spiking when tested with E_{GABA} = -35 mV and -20 mV (p = 1 and 0.40, respectively). Among nerve-injured cells, shifting E_{GABA} from -35 mV to -20 mV significantly increased the proportion with PAD-induced spiking (p = 0.001). Consistent with the combined effects of 4-AP and altered E_{GABA}, the proportion of cells with PAD-induced spiking was most significantly increased by the combination of nerve injury and a depolarizing shift in E_{GABA} ($p < 10^{-5}$).

PAD-induced repetitive spiking in DRG neurons

Testing with current injection (I_{stim}) confirmed that 4-AP had the intended effect of increasing excitability yet, despite responding to I_{stim} steps with repetitive spiking, most neurons responded to g_{GABA} steps with transient spiking, as illustrated in **Fig 3A**. Specifically, PAD-induced repetitive spiking was not observed in any nerve-injured neurons and was seen in only two neurons after 4-AP application. All neurons were tested with a broad range of $\bar{g}_{\text{GABA}}$ to confirm that repetitive spiking could not eventually be achieved by applying a stronger conductance. Increasing $\bar{g}_{\text{GABA}}$ above the minimum required to elicit transient spiking consistently caused attenuation of the spike height and clamped the subsequent voltage near E_{GABA} (**Fig 3B**). Based on our simulation results (see Fig 1A), we reasoned that the lack of repetitive
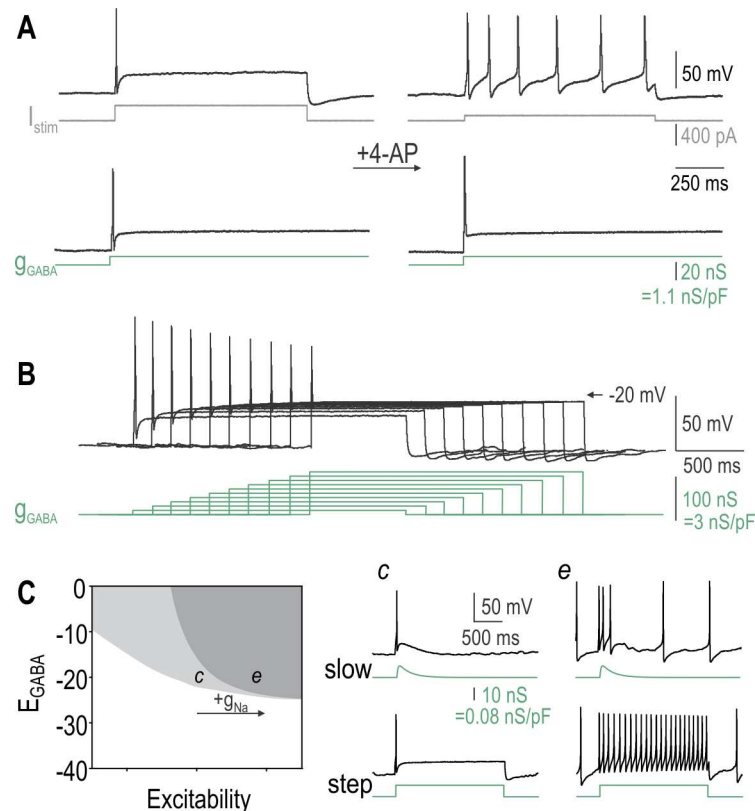
Fig 3. PAD-induced repetitive spiking in DRG neurons. (A) Sample traces from a typical neuron showing that 4-AP had the intended effect of enabling repetitive spiking in response to current injection (I_{stim}, top traces), yet virtual GABA conductance continued to elicit only transient spiking (bottom traces). E_{GABA} = -20 mV. Scale bar for g_{GABA} in all panels show nS before and after normalization by membrane capacitance of the recorded cell. **(B)** Responses from another neuron showing that increasing $\bar{g}_{GABA}$ across a very broad range (an order of magnitude greater than required for transient spiking) failed to eventually induce repetitive spiking. Instead, spike amplitude was attenuated and membrane potential was effectively clamped near E_{GABA} after the initial spike. **(C)** To further increase excitability, dynamic clamp was used to insert a virtual voltage-dependent sodium conductance ($\bar{g}_{Na}$ = 0.2 nS/pF) after applying 4-AP. The effectiveness of this manipulation is clear from the development of spontaneous spiking (right panels). Under these conditions, a slow g_{GABA} waveform or g_{GABA} step induced repetitive spiking. The result was observed in 2 of 2 neurons tested.

doi:10.1371/journal.pcbi.1005215.g003

spiking was due to 4-AP or nerve injury not causing a sufficient increase in excitability. To test this hypothesis, we further increased excitability by using dynamic clamp to introduce a virtual sodium conductance like that upregulated after nerve injury [45]. As predicted, PAD-induced repetitive spiking was made possible by this additional manipulation (Fig 3C). Although we managed to reproduce PAD-induced repetitive spiking, the extent of the required manipulations suggests that naturally occurring pathological changes cause few neurons to become sufficiently hyperexcitable that PAD will induce repetitive spiking. That said, if the central terminals of axons are more excitable (i.e. more prone to repetitive spiking) than the soma, PAD would be more likely to elicit repetitive spiking than suggested by our data.

PAD-mediated inhibition in a model neuron

The above results demonstrate that depolarizing GABA current can induce transient spiking under conditions associated with nerve injury. This does not, however, exclude PAD from

retaining its inhibitory effects, especially given that inhibition stems from sodium channel inactivation and shunting. In fact, although PAD may induce a single spike at its onset, shunting effects persist as long as $GABA_A R$ are activated. This raises the important question of whether more spikes (arising in the periphery or ectopically in the soma or a neuroma) are blocked by PAD than are induced by PAD in the central axon terminals.

Our initial model did not include sodium channel inactivation for the sake of simplicity; therefore, our next step was to modify the model so that a certain proportion of sodium channels, controlled by parameter p, experience inactivation (Eqn. 7). Using this new model, we set β_w to 0 mV to facilitate repetitive spiking and conducted 2-D bifurcation analysis to determine the p and E_{GABA} combinations associated with different effects of PAD (Fig 4A). The grey region shows parameter combinations for which a g_{GABA} step (2 nS/pF) applied alone elicits spiking (sample traces a and d in Fig 4B). The green region shows parameter combinations for which the same g_{GABA} step inhibits spiking induced by I_{stim} steps (sample traces c-e in Fig 4B). Importantly, the green and grey regions overlap, thus demonstrating that PAD can induce spikes yet nonetheless block spikes originating by other means. Fig 4C shows the 2-D bifurcation analysis repeated for different $\bar{g}_{GABA}$ values. The region of PAD-induced spiking remained
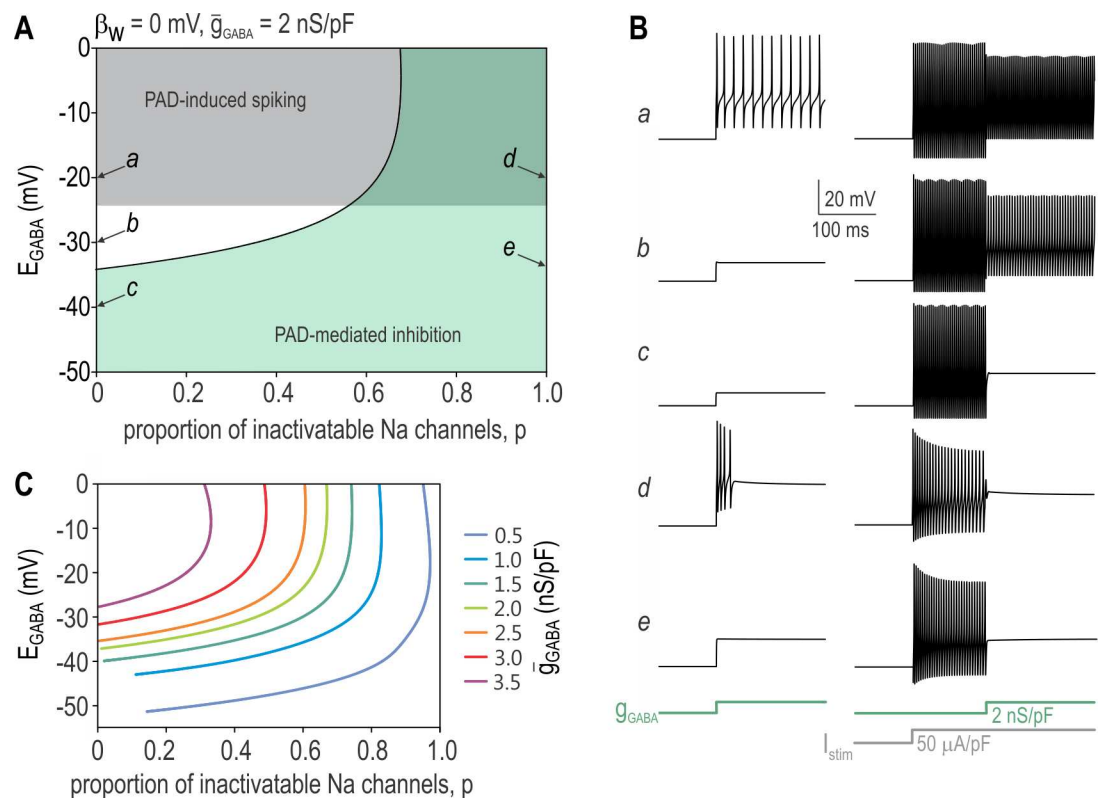

Fig 4. PAD-mediated inhibition in a neuron model. (A) 2-D bifurcation diagram showing the combinations of E_{GABA} and p associated with PAD-induced spiking (grey region) and PAD-mediated inhibition of other spiking (green region), where p represents the proportion of sodium channels susceptible to inactivation. Simulations here are based on a neuron model with sodium channel inactivation (Eq 7) with $\beta_w = 0$ mV and $\bar{g}_{GABA} = 2$ nS/pF. Note that the green and grey regions overlap, indicating that PAD can initiate its own spikes yet still inhibit spikes initiated by other means (e.g. by stimulating current I_{stim}). Labels a-e indicate parameter combinations for which sample responses are shown in B. (B) Responses to g_{GABA} steps occurring alone or during I_{stim} steps are shown down the left and right columns, respectively. (C) Boundary between inhibitory and non-inhibitory region (as in A) re-plotted for different $\bar{g}_{GABA}$. Higher $\bar{g}_{GABA}$ enables GABA to be inhibitory despite less inactivating sodium current (i.e. smaller p) and more depolarized E_{GABA}.

doi:10.1371/journal.pcbi.1005215.g004

unchanged (not illustrated) but the region of PAD-mediated inhibition expanded as $\bar{g}_{GABA}$ was increased, suggesting that stronger $GABA_AR$ activation manages to terminate spiking despite a smaller proportion of inactivatable sodium channels.

PAD-mediated inhibition in DRG neurons

To measure PAD-mediated inhibition in real DRG neurons, we combined g_{GABA} and I_{stim} steps as done for simulations in Fig 4B. Fig 5A shows a typical neuron in which I_{stim} elicited repetitive spiking. Interposing a g_{GABA} step during the I_{stim} step caused reduction or complete cessation of repetitive spiking depending on $\bar{g}_{GABA}$ and E_{GABA}. Note that spikes occurring during the g_{GABA} step were shorter than those occurring outside the g_{GABA} step, consistent with the shunting effect of the virtual GABA conductance. Applying the g_{GABA} step before the onset of I_{stim} confirmed that the former could elicit transient spiking yet still inhibit the repetitive
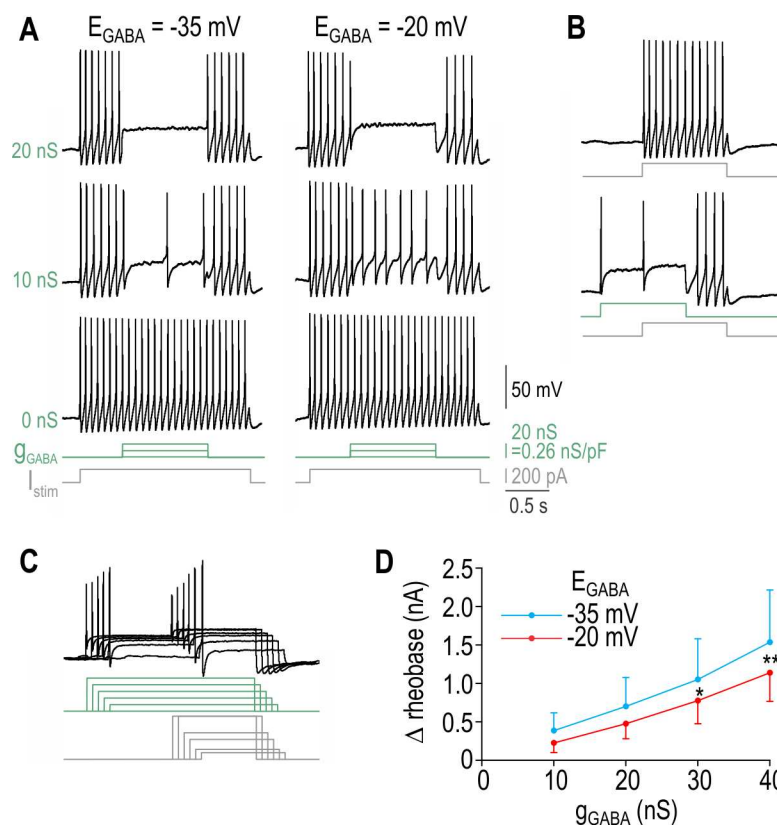

Fig 5. PAD-mediated inhibition in DRG neurons. (A) Sample responses from a typical neuron made hyperexcitable by 4-AP and virtual sodium conductance ($\bar{g}_{Na}$ = 0.3 nS/pF). The repetitive spiking elicited by the I_{stim} step was reduced by application of a small g_{GABA} step (middle row) and was altogether stopped by larger g_{GABA} steps (top row). For equivalent $\bar{g}_{GABA}$, stronger inhibition was evident with E_{GABA} = -35 mV than with E_{GABA} = -20 mV (compare left and right columns). (B) Sequence of I_{stim} and g_{GABA} steps was changed to verify that the latter could elicit transient spiking yet still inhibit the repetitive spiking driven by I_{stim}. Note that repetitive spiking starts after the g_{GABA} step ends and lasts until the I_{stim} step ends. (C) PAD-mediated inhibition of transient spiking was assessed using the same protocol as in B but we varied the amplitude of the I_{stim} step to determine rheobase (i.e. the minimum I_{stim} required to evoke spiking). Only responses to rheobasic stimulation are shown. Note that rheobase increases with increases in $\bar{g}_{GABA}$, whereas spike height decreases. (D) Change in rheobase (mean ± SEM) is plotted against $\bar{g}_{GABA}$ for E_{GABA} = -35 mV (blue, n = 3 cells) and -20 mV (red, n = 4 cells). Rheobase was significantly increased by $\bar{g}_{GABA}$ (p = 0.013, one-way repeated measures ANOVA; p = 0.013 (*), p = 0.002 (**), Holm-Sidak post-hoc tests vs no g_{GABA}) but E_{GABA} did not have a significant effect (p = 0.52).

doi:10.1371/journal.pcbi.1005215.g005

spiking otherwise driven by I_{stim} (**Fig 5B**). Using the same stimulus sequence, we measured rheobase (i.e. the minimum I_{stim} required to elicit spiking) for each level of $\bar{g}_{GABA}$ (**Fig 5C**). Rheobase was significantly increased by increments in $\bar{g}_{GABA}$ ($p = 0.013$, two-way repeated measures ANOVA) but was not significantly affected by E_{GABA} ($p = 0.52$) (**Fig 5D**). These data confirm that PAD elicited in the cell body of DRG neurons mediates shunting inhibition even under conditions in which it can induce spiking.

Possible involvement of calcium-activated chloride channels in PAD

Activation of the calcium-activated chloride channel ANO-1 in primary afferent neurons can evoke or exacerbate pain, especially under inflammatory or neuropathic conditions [47–50]. Notably, intracellular chloride tends to be elevated under those conditions (see Introduction), which may explain why ANO-1 activation is excitatory rather than inhibitory. Consistent with this, ANO-1 modulation of spiking evoked by current injection is sensitive to intracellular chloride level [51] but demonstration that ANO-1 itself evokes spiking was based on a chloride reversal potential of -18 mV [49]. Given its activation requirements [52], we predicted that ANO-1 channels would not be activated by the GABAergic input underlying PAD; recall that $GABA_A R$ activation is necessary for PAD [22]. Nonetheless, to rule out a contribution by ANO-1, we repeated virtual PAD experiments (like in Fig 2) before and after blockade of ANO-1 channels by bath-applied 10 μM T16Ainh-A01 (A01) (**Fig 6**). Based on the pipette solution, the chloride reversal potential for ANO-1 was -20 mV but E_{GABA} for virtual g_{GABA} was set to -35 or -20 mV in dynamic clamp. As predicted, ANO-1 blockade had no significant effect on the minimum $\bar{g}_{GABA}$ needed to evoke spiking for E_{GABA} = -20 mV ($p = 1.0$, paired t-test; **Fig 6A**) and nor did it significantly affect the depolarization evoked by different $\bar{g}_{GABA}$ for E_{GABA} = -35 mV ($p = 0.77$, two-way repeated measures ANOVA; **Fig 6B**) or have any effect on rheobase, input resistance, or resting membrane potential ($p > 0.05$, paired t-tests). The data above are based exclusively on capsaicin-responsive cells (see **Fig 6C**) since ANO-1 channels are expressed primarily in cells that express TRPV1 [47]. Notably, the response to capsaicin was reduced by ANO-1 blockade (**Fig 6D**), consistent with Takayama et al. [49] and thus verifying the efficacy of our A01. Based on these results, we conclude that ANO-1 channels are not activated and, therefore, do not contribute to PAD under our experimental conditions.

PAD-mediated inhibition of spike propagation in a multicompartment model neuron

All simulations described thus far were conducted in a single compartment model. This adequately simulates spike initiation occurring in proximity to the recording electrode, as occurs when recording from an isolated DRG soma. Although spontaneous or PAD-induced spiking may arise at the site of PAD, an important inhibitory effect of PAD in the intact fiber is to block the orthodromic propagation of spikes originating in the periphery. To test for conduction block, we converted our single-compartment model into a 3-compartment model (**Fig 7A**). Although still very simple compared with past models used to study this topic [e.g. 19,25,53], this model suffices to qualitatively illustrate key points relevant for the present study. Each compartment was further subdivided into equipotential segments. Based on its small diameter and the absence of nodes, this model simulates continuous propagation in an unmyelinated fiber. By applying GABA conductance to the middle compartment, we tested if that conductance can induce spikes (originating within that compartment) and/or block the propagation of other spikes (evoked at the far end of adjacent compartment).

For an E_{GABA} value of -35 mV, g_{GABA} never evoked spiking (consistent with the single-compartment model) but it did block spike propagation (**Fig 7B**, left column). Interestingly,
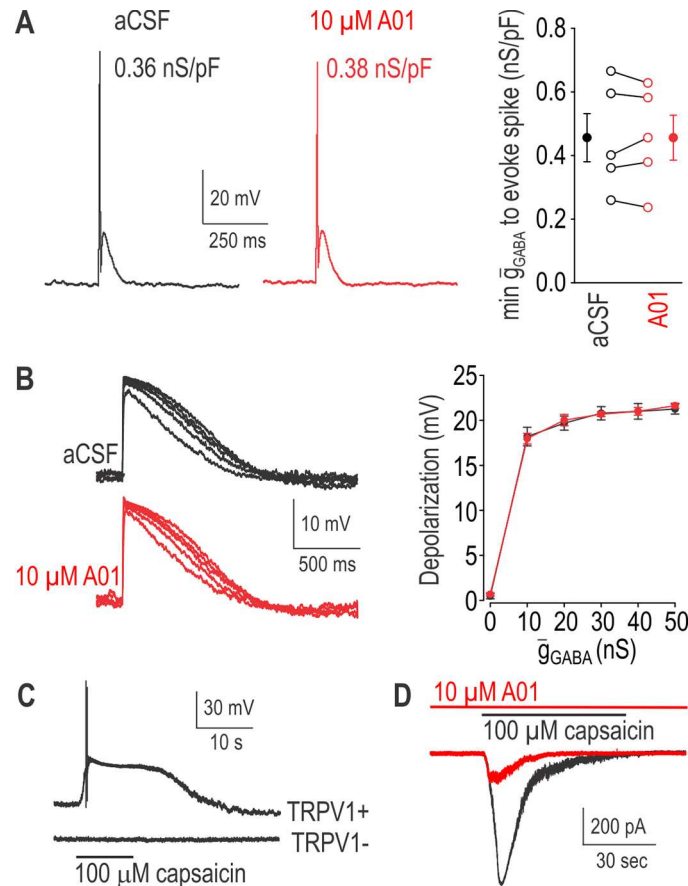
Fig 6. ANO-1 channels do not contribute to PAD. For all panels, responses in the presence of the ANO-1 antagonist T16Ainh-A01 (A01) are shown in red for comparison against responses in normal aCSF shown in black. **(A)** Traces show responses in a typical neuron to the minimum virtual $\bar{g}_{GABA}$ required to evoke spiking based on a fast synaptic waveform and E_{GABA} = -20 mV before and after ANO-1 blockade. Summary data show that the minimum $\bar{g}_{GABA}$ to evoke spiking was not significantly changed by A01 (p = 1.0; paired t-test) based on all TRPV1+ neurons (n = 5) that spiked in response to virtual GABA. **(B)** Traces show responses in a typical neuron to different $\bar{g}_{GABA}$ based on slow synaptic waveform and E_{GABA} = -35 mV. Summary data show mean (± SEM) depolarization at different $\bar{g}_{GABA}$ for all (n = 7) TRPV1+ neurons tested. Blockade of ANO-1 did not significantly affect depolarization (p = 0.77; two-way repeated measure ANOVA). **(C)** At the end of each experiment, the recorded cell was stimulated with capsaicin. Traces show typical data from a responsive (TRPV1+) and unresponsive (TRPV1-) neuron. Because ANO-1 is expressed predominantly in TRPV1+ neurons, only data from capsaicin-responsive neurons were included for analysis in panels A and B. **(D)** To confirm the efficacy A01, we verified that it reduced the response to capsaicin, consistent with Takayama et al. [49].

doi:10.1371/journal.pcbi.1005215.g006

blocked propagation could occur even in the absence of sodium channel inactivation, therein supporting claims that shunting mediated by g_{GABA} mediates an inhibitory effect. When E_{GABA} was shifted to -20 mV, g_{GABA} evoked a single spike that propagated in both directions away from the center compartment (**Fig 7B**, right column). Yet despite this excitatory effect, propagation of other spikes was blocked in two of the three conditions illustrated. Sample traces were chosen to illustrate that large g_{GABA} could block propagation in the absence of sodium channel inactivation but a smaller g_{GABA} could achieve the same effect when combined with sodium channel inactivation. **Fig 7C** demonstrates that sodium channel inactivation can accumulate over time, thus eventually blocking spikes traveling as part of a train. These results confirm that PAD does not abruptly lose its inhibitory effects once able to induce its own spikes.
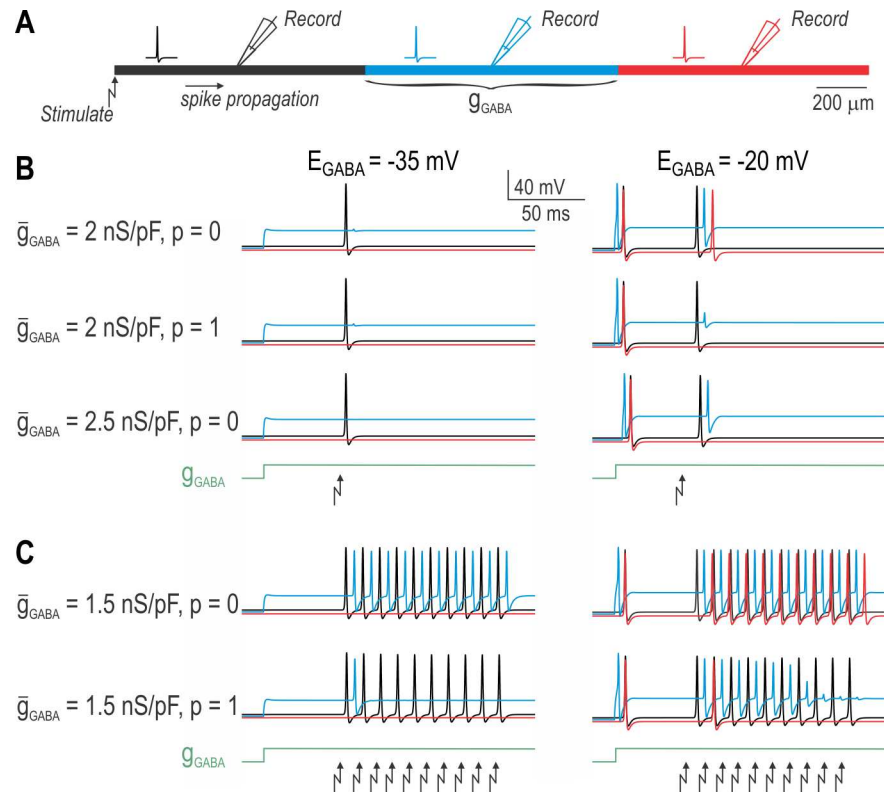
Fig 7. PAD-mediated inhibition of spike propagation in a multi-compartment axon model. (A) Cartoon depicts our three-compartment axon model. One or more spikes were initiated by current injection applied to the left end of the axon. Voltage was measured at the midpoint of each compartment; color of traces in B and C correspond to compartment colors shown in A. GABA conductance was distributed uniformly throughout the middle (blue) compartment. **(B)** For E_{GABA} = -35 mV (left column), g_{GABA} blocked the propagation of the evoked spike under all three combinations of $\bar{g}_{GABA}$ and p that were tested, where p represents the proportion of sodium channels susceptible to inactivation. The g_{GABA} step did not elicit its own spiking in any condition. On the other hand, for E_{GABA} = -20 mV (right column), PAD-induced transient spiking was observed for all three conditions yet propagation of the stimulus-evoked spike was blocked in two of the three conditions. Comparing the top and middle panels shows that modest $\bar{g}_{GABA}$ relies on sodium channel inactivation to block spike propagation, whereas stronger $\bar{g}_{GABA}$ could block propagation without any contribution from sodium channel inactivation. **(C)** During a spike train, sodium channel inactivation accumulates between spikes such that spikes early in the train can propagate whereas later spikes do not. Comparing with combinations of $\bar{g}_{GABA}$ and p required to block propagation of a single spike (see B), these results show that partial blockade during a spike train can be mediated by even comparatively weak PAD.

doi:10.1371/journal.pcbi.1005215.g007

Discussion

Using computer simulations and an experimental approach distinct from previous studies, we have identified which pathological changes are necessary and sufficient to enable PAD-induced spiking. We determined that a depolarizing shift in E_{GABA} is necessary yet insufficient to enable PAD-induced spiking in most DRG neurons. An increase in intrinsic excitability (i.e. altered spike initiation properties) is also necessary, especially to enable PAD-induced repetitive spiking. Neurons may experience both changes after nerve injury or inflammation, meaning PAD-induced spiking could occur in certain pathological conditions [22,26,29]; however, other factors such as the requirement for fast depolarization suggest that PAD-induced spiking is probably rare (see below), but this depends on the excitability of central axon terminals, which still remains uncertain. Intriguingly, our data also suggest that PAD continues to mediate presynaptic inhibition under conditions in which it can induce transient spiking. Although seemingly

paradoxical, the co-existence of excitatory and inhibitory effects has been observed previously in studies of presynaptic inhibition in crayfish [54] and is consistent with the biophysical mechanisms responsible for each effect. This is unlike what happens postsynaptically in spinal neurons, where paradoxical excitation develops only after inhibition fails [10,55]. Our data argue that increased PAD has a net inhibitory effect, meaning paradoxical excitation via enhanced PAD poses less risk to somatosensory processing than disinhibition caused by reduced PAD.

The GABA conductance density required for PAD-induced spiking under normal conditions is evidently quite high, so much so that we were able to elicit spiking in only 2 of 29 neurons despite testing with virtual $\bar{g}_{GABA}$ several times greater than the typical density measured in somata [13,35]. This is consistent with previous failures to elicit spikes by puffing GABA on the soma [13,35,42]. Puffed GABA also failed to elicit calcium signals when applied to the central terminals of GCaMP-expressing primary afferents [13], and Verdier et al. [56] observed GABA-induced spiking in only 4 of 77 neurons tested in the trigeminal nucleus. The value of $\bar{g}_{GABA}$ in central axon terminals remains an open question but evidence points to reduced expression of presynaptic GABA$_A$Rs following nerve injury [13,57,58], which suggests that presynaptic inhibition is weakened by reduction of $\bar{g}_{GABA}$ rather than $\bar{g}_{GABA}$ becoming strong enough that PAD induces spiking. That said, the minimum $\bar{g}_{GABA}$ needed for PAD-induced spiking is reduced by increased neuronal excitability (**Fig 2C**) and by a depolarizing shift in E_{GABA} (**Fig 2D**). Unlike an increase in $\bar{g}_{GABA}$, which increases inhibitory effects due to shunting, increased neuronal excitability and depolarized E_{GABA} can encourage PAD-induced spiking without enhancing PAD-mediated shunting. Studying transient spiking cells in the chick cochlear nucleus, Monsivais and Rubel [59] found that depolarizing GABA$_A$R input could elicit spiking after blockade of the low-threshold potassium current known to be responsible for transient spiking [60]. The same GABA$_A$R input normally inhibited stimulus-evoked spiking by activating the low-threshold potassium current and thereby elevating spike threshold [59]. Those data are entirely consistent with results presented here. Notably, PAD-induced spiking would be more likely in central axon terminals if those terminals are more excitable that we have assumed based on extrapolation from somatic data.

Intracellular chloride *could* be depleted during PAD if chloride uptake via NKCC1 became saturated (at least transiently) and thus failed to keep pace with chloride efflux via activated GABA$_A$ channels. The potential for altered chloride concentration is exacerbated by the small caliber of central axon terminals, especially C fibers, since intracellular volume is small compared to surface area [61]. Chloride depletion, if it occurred, would cause an activity-dependent hyperpolarizing shift in E_{GABA}, the implication being that E_{GABA} may be near -20 mV only at the onset of GABA$_A$R activation. Given that PAD-induced spiking depends on a depolarized E_{GABA} value, a hyperpolarizing shift would discourage PAD-induced repetitive spiking. That said, the transient spiking observed in our dynamic clamp experiments was not due to chloride depletion since the virtual GABA current is mediated by current injection through the patch pipette rather than by chloride efflux across the cell membrane. In effect, PAD-induced repetitive spiking may be more difficult to evoke under natural conditions, and transient spiking may rely even more heavily on abrupt depolarization than our experiments suggest.

Following on the above points, both simulations and experiments demonstrated that smaller pathological changes in E_{GABA} and/or excitability are required to enable PAD-induced transient spiking than are required for PAD-induced repetitive spiking. This has important implications. Even if sustained, PAD is likely to produce only one spike at its onset (if it produces any spikes at all) and will likely not produce any spikes unless its onset is abrupt. This is because transient spiking involves a spike initiation mechanism that is sensitive to the rate of depolarization [40]. Sensitivity to g_{GABA} onset kinetics would be inconsequential if presynaptic

inhibition was phasic, which is to say that the $GABA_A$Rs are clustered within the synaptic cleft and therefore receive an abrupt pulse of GABA upon its vesicular release [62], but evidence points toward a more tonic mode of action (unlike the phasic inhibition studied in the crayfish neuromuscular junction [63]) as outlined below. Recording from mammalian primary afferent terminals to measure the activation kinetics (and density) of the $GABA_A$R current is prohibitively difficult, but immunocytochemical evidence argues that C fiber terminals are devoid of gephyrin [64]. Since gephyrin is usually necessary for $GABA_A$R clustering [65], its absence suggests that $GABA_A$Rs are distributed more diffusely. Electrophysiological evidence for high-affinity $GABA_A$Rs in primary afferent neurons [37] supports this view since such receptors have a δ subunit [66] in place of the γ subunit that is necessary for clustering [62,67]. If primary afferent $GABA_A$Rs are indeed distributed extrasynaptically, and are thus activated asynchronously as GABA diffuses beyond the synaptic cleft, then g_{GABA} will have slow onset kinetics and is unlikely to elicit transient spiking. Only the most hyperexcitable fibers (i.e. those capable of PAD-induced repetitive spiking) are likely to exhibit any PAD-induced spiking. And whereas PAD-induced transient spiking relies on abrupt $GABA_A$R activation, PAD-mediated inhibition does not; instead, PAD-mediated inhibitory effects will last throughout the duration of the PAD. In other words, slow activation of extrasynaptic $GABA_A$Rs–arguably the most likely scenario at least for C fiber terminals (see above)–will not cause PAD-induced spiking but will cause PAD-mediated inhibition.

Notably, dorsal root reflexes (DRRs) have typically been studied using electrical stimulation of a nerve or dorsal root to synchronously activate a large number of afferent fibers [e.g. 68]. Notwithstanding differential conduction latencies, such input will evoke a large burst of GABA release, causing $GABA_A$R activation that is ideally suited for PAD-induced transient spiking. It is not obvious that those same fibers would exhibit PAD-induced spiking under more natural conditions (i.e. less synchronous inputs). However, Dubuc et al. [69] observed antidromic spiking in 19% of cat dorsal root fibers during fictive locomotion. It has long been recognized that dorsal root reflexes are more common in certain afferents (e.g. stretch receptors) with direct evidence for DRRs being weakest in C fibres [22]. However, Lin et al. [36] reported spontaneous and von Frey-evoked antidromic spiking in all fiber types and, moreover, found that intradermal capsaicin selectively increased antidromic spiking in C and Aδ fibers. Based on more recent observations, including data presented here, one may suspect that chloride regulation, GABA receptor clustering and/or intrinsic excitability differ between afferent types. Somatic recordings suggest that important differences do indeed exist [70] but definitively resolving this requires comparison of axon terminals (rather than somata) and is therefore technically difficult. Notably, Dubuc et al. [69] observed repetitive antidromic spiking, as have others [e.g. 71], which argues that the excitability of certain afferent terminals is quite high. The role of axonal excitability warrants closer attention in future studies. Observation that cooling increases DRRs [72] likely holds important clues. Please see [5] for a recent review of other factors.

As already explained, PAD-induced spiking does not equate with failure of presynaptic inhibition. The resilience of presynaptic inhibition is best appreciated by comparing how pre- and postsynaptic inhibition fail. As KCC2 is downregulated postsynaptically, E_{GABA} undergoes a depolarizing shift that directly compromises the inhibitory effect of GABAergic input [61]. The same shift in E_{GABA} that reduces postsynaptic inhibition is what eventually results in paradoxical excitation. This shift from inhibition to paradoxical excitation is evidently not what happens presynaptically. In primary afferent terminals, the changes required for paradoxical excitation–a shift in E_{GABA} and increased excitability–do not undermine the inhibitory effect; in fact, the relatively high $\bar{g}_{GABA}$ required for PAD-induced spiking also encourages PAD-mediated inhibition. This conclusion contradicts past assumptions on this matter. Furthermore, whereas the risk of paradoxical excitation increases postsynaptically during sustained GABAergic input (because of

chloride accumulation), presynaptically, the balance shifts towards inhibitory effects over time as sodium channel inactivation accumulates and if intracellular chloride is depleted. The greatest risk to presynaptic inhibition is reduced PAD rather than enhanced PAD.

To conclude, we have demonstrated that combined changes in E_{GABA} and intrinsic excitability enable PAD-induced transient spiking. However, unless neurons become so hyperexcitable that PAD can induce repetitive spiking, slow (asynchronous) activation of extrasynaptic GABA$_A$Rs is unlikely to elicit any spiking. On the other hand, PAD will continue to mediate presynaptic inhibition. In practical terms, our results suggest that presynaptic inhibition is a viable therapeutic target whose enhancement carries little risk of causing paradoxical excitation.

Methods

Ethics Statement

All experiments were approved by the University of Pittsburgh IACUC and by The Hospital for Sick Children Animal Care Committee.

Computer simulations

Starting from a previously published model [45,73], our single compartment, conductance-based model is described as follows:

$$C \frac{dV}{dt} = I_{\text{stim}} - \bar{g}_{\text{Na}} m_\infty(V)(V - E_{Na}) - \bar{g}_{\text{K}} w(V - E_{\text{K}}) - g_{\text{leak}}(V - E_{\text{leak}}) - g_{\text{GABA}}(t)(V - E_{\text{GABA}}) \quad (1)$$

where activation variable m changes instantaneously with voltage V according to

$$m_\infty(V) = 0.5 \left[1 + \tanh\left(\frac{V - \beta_{\text{m}}}{\gamma_{\text{m}}} \right) \right], \quad (2)$$

whereas w changes more slowly according to

$$\frac{dw}{dt} = \phi_{\text{w}} \frac{w_\infty(V) - w}{\tau_w(V)}, \quad (3)$$

$$w_\infty(V) = 0.5 \left[1 + \tanh\left(\frac{V - \beta_{\text{w}}}{\gamma_{\text{w}}} \right) \right], \quad (4)$$

$$\tau_w(V) = \frac{1}{\cosh\left(\frac{V - \beta_{\text{w}}}{2\gamma_{\text{w}}} \right)}. \quad (5)$$

Neuronal excitability was varied by changing parameter β_{w} [38]. Injury-induced hyperexcitability can be reproduced by shifting β_{w} from its normal value of around -20 mV to less negative values [73]. Setting β_{w} to less negative values reflects a multitude of potential injury-induced molecular changes including reduced K$_V$1-type potassium current, which we model experimentally using 4-AP application, and increased sodium current, which we model experimentally using dynamic clamp (see below); the effect of such changes, occurring alone or together, is to alter spike initiation [45]. All other neuronal parameters were fixed as reported previously [38] at the following values: C = 2 μF/cm^2; sodium conductance $\bar{g}_{\text{Na}}$ = 20 mS/cm^2, E_{Na} = 50 mV, β_{m} = -1.2 mV, γ_{m} = 18 mV; potassium conductance $\bar{g}_{\text{K}}$ = 20 mS/cm^2, E_{K} = -100 mV, ϕ_w = 0.15, γ_{w} = 10 mV; leak conductance g_{leak} = 2 mS/cm^2, E_{leak} = -70 mV.

Stimulating current I_{stim} was not applied unless indicated. Maximal GABA conductance density $\bar{g}_{\text{GABA}}$ and reversal potential E_{GABA} were varied. Units for $\bar{g}_{\text{GABA}}$ were converted to nS/

pF for comparison with experimental measurements. The normal E_{GABA} value in primary afferent is around -35 mV based on measurements using different techniques [12,13,35,42]. GABA conductance was activated as a step or as a synaptic waveform described by

$$g_{GABA}(t) = \bar{g}_{GABA} x \left[-e^{-t/\tau_{rise}} + e^{-t/\tau_{decay}} \right], \tag{6}$$

which comprises an exponential rise to maximum (with time constant τ_{rise}) followed by an exponential decay back to baseline (with τ_{decay}). The peak is normalized to 1 by factor x before being scaled by $\bar{g}_{GABA}$. Kinetics are reported in the Results section.

For simulations reported in Figs 4 and 7, sodium channel inactivation h was applied to a proportion of sodium channels defined by p, thus giving the following current balance equation

$$C \frac{dV}{dt} = I_{stim} - p\,\bar{g}_{Na}m_{\infty}(V)h(V - E_{Na}) - (1-p)\,\bar{g}_{Na}m_{\infty}(V)(V - E_{Na}) - \bar{g}_{K}w(V - E_{K})$$
$$- g_{leak}(V - E_{leak}) - g_{GABA}(t)(V - E_{GABA}). \tag{7}$$

Changes in h are described by the same equations used to describe w (Eq 3–5) where β_{h} = -28 mV, γ_{h} = -14 mV, and ϕ_{h} = 0.005.

All simulations in single compartment models were conducted in XPP. Bifurcation analysis was conducted using AUTO via the XPP interface. The multicompartment model was built in NEURON. Ion channels were modeled as above except that both $\bar{g}_{Na}$ and $\bar{g}_{K}$ were increased to 30 mS/cm². Additional parameters were as follows: axial resistivity R_{a} = 150 Ω·cm, diameter = 1 μm, compartment length = 1 mm, d_lambda = 0.01. GABA conductance $\bar{g}_{GABA}$ was modeled as a uniform density throughout the middle compartment.

Dorsal root ganglion (DRG) neuron preparation and electrophysiology

All experiments were carried out on adult (200–340 g) male Sprague-Dawley rats (Harlan, Indianapolis, IN and Charles River, Montreal, Quebec). A subset of animals received spinal nerve ligation (SNL) 2–5 days before terminal experiments [74]. Under isoflurane anesthesia, the paraspinal muscles were separated to access the L6 process, which was carefully removed. The L5 spinal nerve was tightly ligated with 6–0 silk suture. All nerve-injured animals maintained motor function but developed neuropathic pain as inferred by guarding of the affected paw.

To collect DRG neurons, rats were deeply anesthetized by subcutaneous injection of anesthetic cocktail (1 ml/kg of 55 mg/ml ketamine, 5.5 mg/ml xylazine, and 1.1 mg/ml acepromazine) or by isoflurane (4% for induction; 2.5% for maintenance). DRG (L4 and L5 in naïve animals; L5 in nerve-injured animals) were surgically removed to chilled MEM-FBS culture media and desheathed. DRG were then enzymatically treated for 45 minutes in culture media composed of 89% MEM, 370 units/ml penicillin and 370 μg/ml streptomycin, 1% MEM vitamin solution (all from Life Technologies), and 1.2 mg/ml collagenase Type 4 (Worthington Biochemical Corp). DRG were mechanically dissociated by trituration with a fire-polished Pasteur pipette, and further enzymatically treated for 5 minutes in Ca^{2+}- and Mg^{2+}-free Hanks' balanced salt solution (HBSS; Life Technologies Inc), containing 2.5 mg/ml trypsin (Worthington Biochemical Corp) and 0.02% sterile ethylenediaminetetraacetic acid (EDTA; Sigma-Aldrich Canada Ltd). Trypsin activity was subsequently inhibited by the addition of MEM-FBS supplemented with 0.625 mg/ml $MgSO_4$ (Caledon Labs). Dissociated cells in MEM-FBS were plated on glass coverslips previously coated by a solution of 0.1 mg/ml poly-D-lysine, and incubated in MEM-FBS at 37°C, 5% CO_2, and 90% humidity for 2 h. Coverslips were then

transferred to a HEPES-buffered Leibovitz's L-15 media containing glutamine (Life Technologies Ltd), 10% FBS, 100 units/ml of penicillin and 100 μg/ml streptomycin, and 5 mM D-glucose (Caledon Labs) and stored at room temperature until used for experiments for 2–28 hours later. Spiking properties do not change appreciably over this period and nor do neurites develop based on storage at room temperature, omission of laminin from coverslips, and the growth factor-free culture medium used.

Coverslips with cultured cells were transferred to a recording chamber constantly perfused with room temperature, oxygenated (95% O_2 and 5% CO_2) artificial cerebral spinal fluid containing (in mM) 126 NaCl, 2.5 KCl, 2 $CaCl_2$, 2 $MgCl_2$, 10 D-glucose, 26 $NaHCO_3$, 1.25 NaH_2PO_4. Cells were recorded in the whole-cell configuration with >70% series resistance compensation using an Axopatch 200B amplifier (Molecular Devices; Palo Alto, CA). Electrodes (2–5 MΩ) were filled with a recording solution containing (in mM) 125 $KMeSO_4$, 5 KCl, 10 HEPES, 2 $MgCl_2$, 4 ATP, 0.4 GTP as well as 0.1% Lucifer Yellow; pH was adjusted to 7.2 with KOH and osmolality was between 270 and 290 mosmol/L. For experiments on the contribution of ANO-1 channels, $KMeSO_4$ was reduced to 67 mM and KCl was increased to 63 mM to give E_{Cl} = -20 mV. Data were low-pass filtered at 2 KHz, digitized at 20 KHz using a CED 1401 computer interface (Cambridge Electronic Design, Cambridge, UK), and analyzed offline. Virtual GABA conductance was applied via dynamic clamp using Signal 5 software (CED). The virtual conductance was modeled as a step or as a synaptic waveform described by Eqn. 6. To express the virtual conductance as a density and thus exclude direct effects of cell size, we normalized absolute conductance values by membrane capacitance C because C is proportional to the surface area of the cell. Capacitance was measured for each cell based on responses to small (50 pA) hyperpolarizing current steps, where $C = \tau_{membrane} / R_{in}$. To increase cellular excitability in neurons from naïve animals, potassium channels were blocked with bath applied 4-aminopyridine (4-AP). In a subset of experiments with 4-AP, a virtual voltage-dependent sodium conductance was also inserted via dynamic clamp using the equations and parameters reported by Ratté et al. [45]. Neurons from nerve-injured animals are already hyperexcitable and were not, therefore, subject to manipulations (i.e. 4-AP or virtual sodium conductance) intended to increase excitability.

All data and computer code are available from the corresponding author upon request.

Supporting Information

S1 Fig. The neuron model used in Fig 1 was modified to reproduce the minimum $\bar{g}_{GABA}$ required to evoke spiking observed experimentally in Fig 2. Specifically, we reduced the leak conductance g_{leak} to 0.7 mS/cm^2 and increased the potassium conductance $\bar{g}_K$ to 30 mS/cm^2. All other parameters were unchanged. Testing with different $\bar{g}_{GABA}$ (indicated on the figure), E_{GABA} and β_w were systematically varied like in Fig 1. Labels *a-d* are shown on top of graph shading, which depicts the distribution of excitability that could be expected within a heterogeneous population of neurons. Curves here show the minimum requirements for transient spiking. Note that for low values of $\bar{g}_{GABA}$, a small increase in $\bar{g}_{GABA}$ causes a large shift in the curves, whereas for high values of $\bar{g}_{GABA}$, a large increase in $\bar{g}_{GABA}$ causes little if any shift. Consistent with Fig 1, this re-affirms that increasing $\bar{g}_{GABA}$ will not eventually cause spiking (depending on E_{GABA} and intrinsic neuronal excitability).
(TIF)

Acknowledgments

Author Contributions

Conceptualization: PT YZ SAP.

Formal analysis: PT YZ SAP.

Funding acquisition: SAP.

Investigation: PT YZ SAP.

Methodology: PT YZ SAP.

Project administration: SAP.

Supervision: SAP.

Visualization: PT YZ SAP.

Writing – original draft: PT YZ SAP.

Writing – review & editing: PT YZ SAP.

References

1. Price TJ, Cervero F, Gold MS, Hammond DL, Prescott SA (2009) Chloride regulation in the pain pathway. Brain Res Rev 60: 149–170. doi: 10.1016/j.brainresrev.2008.12.015 PMID: 19167425

2. Zeilhofer HU, Wildner H, Yevenes GE (2012) Fast synaptic inhibition in spinal sensory processing and pain control. Physiol Rev 92: 193–235. doi: 10.1152/physrev.00043.2010 PMID: 22298656

3. Prescott SA (2015) Synaptic inhibition and disinhibition in the spinal dorsal horn. In: Price TJ, Dussor G, editors. Molecular Biology of Pain, Progress in Molecular and Translational Science: Elsevier.

4. Kaila K, Price TJ, Payne JA, Puskarjov M, Voipio J (2014) Cation-chloride cotransporters in neuronal development, plasticity and disease. Nat Rev Neurosci 15: 637–654. doi: 10.1038/nrn3819 PMID: 25234263

5. Guo D, Hu J (2014) Spinal presynaptic inhibition in pain control. Neuroscience 283: 95–106. doi: 10.1016/j.neuroscience.2014.09.032 PMID: 25255936

6. Sorkin LS, Puig S (1996) Neuronal model of tactile allodynia produced by spinal strychnine: effects of excitatory amino acid receptor antagonists and a mu-opiate receptor agonist. Pain 68: 283–292. PMID: 9121816

7. Yaksh TL (1989) Behavioral and autonomic correlates of the tactile evoked allodynia produced by spinal glycine inhibition: effects of modulatory receptor systems and excitatory amino acid antagonists. Pain 37: 111–123. PMID: 2542867

8. Sivilotti L, Woolf CJ (1994) The contribution of GABA(A) and glycine receptors to central sensitization: disinhibition and touch-evoked allodynia in the spinal cord. JNeurophysiol 72: 169–179.

9. Sherman SE, Loomis CW (1994) Morphine insensitive allodynia is produced by intrathecal strychnine in the lightly anesthetized rat. Pain 56: 17–29. PMID: 8159438

10. Coull JA, Boudreau D, Bachand K, Prescott SA, Nault F, et al. (2003) Trans-synaptic shift in anion gradient in spinal lamina I neurons as a mechanism of neuropathic pain. Nature 424: 938–942. doi: 10.1038/nature01868 PMID: 12931188

11. Lucas O, Hilaire C, Delpire E, Scamps F (2012) KCC3-dependent chloride extrusion in adult sensory neurons. Molecular and cellular neurosciences 50: 211–220. doi: 10.1016/j.mcn.2012.05.005 PMID: 22609694

12. Mao S, Garzon-Muvdi T, Di Fulvio M, Chen Y, Delpire E, et al. (2012) Molecular and functional expression of cation-chloride cotransporters in dorsal root ganglion neurons during postnatal maturation. J Neurophysiol 108: 834–852. doi: 10.1152/jn.00970.2011 PMID: 22457464

13. Chen JT, Guo D, Campanelli D, Frattini F, Mayer F, et al. (2014) Presynaptic GABAergic inhibition regulated by BDNF contributes to neuropathic pain induction. Nature communications 5: 5331. doi: 10.1038/ncomms6331 PMID: 25354791

14. Witschi R, Punnakkal P, Paul J, Walczak JS, Cervero F, et al. (2011) Presynaptic alpha2-GABAA receptors in primary afferent depolarization and spinal pain control. J Neurosci 31: 8134–8142. doi: 10.1523/JNEUROSCI.6328-10.2011 PMID: 21632935

15. Sung KW, Kirby M, McDonald MP, Lovinger DM, Delpire E (2000) Abnormal GABAA receptor-mediated currents in dorsal root ganglion neurons isolated from Na-K-2Cl cotransporter null mice. J Neurosci 20: 7531–7538. PMID: 11027211

16. Rocha-Gonzalez HI, Mao S, Alvarez-Leefmans FJ (2008) Na+,K+,2Cl- cotransport and intracellular chloride regulation in rat primary sensory neurons: thermodynamic and kinetic aspects. J Neurophysiol 100: 169–184. doi: 10.1152/jn.01007.2007 PMID: 18385481

17. Alvarez-Leefmans FJ, Gamino SM, Giraldez F, Nogueron I (1988) Intracellular chloride regulation in amphibian dorsal root ganglion neurones studied with ion-selective microelectrodes. J Physiol 406: 225–246. PMID: 3254412

18. Kullmann DM, Ruiz A, Rusakov DM, Scott R, Semyanov A, et al. (2005) Presynaptic, extrasynaptic and axonal GABAA receptors in the CNS: where and why? Progress in biophysics and molecular biology 87: 33–46. doi: 10.1016/j.pbiomolbio.2004.06.003 PMID: 15471589

19. Graham B, Redman S (1994) A simulation of action potentials in synaptic boutons during presynaptic inhibition. J Neurophysiol 71: 538–549. PMID: 8176423

20. Willis WD (2006) John Eccles' studies of spinal cord presynaptic inhibition. Prog Neurobiol 78: 189–214. doi: 10.1016/j.pneurobio.2006.02.007 PMID: 16650518

21. MacDermott AB, Role LW, Siegelbaum SA (1999) Presynaptic ionotropic receptors and the control of transmitter release. AnnuRevNeurosci 22: 443–485.

22. Willis WD Jr. (1999) Dorsal root potentials and dorsal root reflexes: a double-edged sword. Exp Brain Res 124: 395–421. PMID: 10090653

23. Gossard JP, Bouyer L, Rossignol S (1999) The effects of antidromic discharges on orthodromic firing of primary afferents in the cat. Brain Res 825: 132–145. PMID: 10216180

24. Bevengut M, Clarac F, Cattaert D (1997) Antidromic modulation of a proprioceptor sensory discharge in crayfish. J Neurophysiol 78: 1180–1183. PMID: 9307148

25. Lamotte d'Incamps B, Meunier C, Monnet ML, Jami L, Zytnicki D (1998) Reduction of presynaptic action potentials by PAD: model and experimental study. JComputNeurosci 5: 141–156.

26. Cervero F, Laird JM (1996) Mechanisms of touch-evoked pain (allodynia): a new model. Pain 68: 13–23. PMID: 9251994

27. Rees H, Sluka KA, Westlund KN, Willis WD (1995) The role of glutamate and GABA receptors in the generation of dorsal root reflexes by acute arthritis in the anaesthetized rat. J Physiol 484 (Pt 2): 437–445.

28. Valencia-de Ita S, Lawand NB, Lin Q, Castaneda-Hernandez G, Willis WD (2006) Role of the Na+-K+-2Cl- cotransporter in the development of capsaicin-induced neurogenic inflammation. J Neurophysiol 95: 3553–3561. doi: 10.1152/jn.01091.2005 PMID: 16709721

29. Cervero F, Laird JM, Garcia-Nicas E (2003) Secondary hyperalgesia and presynaptic inhibition: an update. EurJ Pain 7: 345–351.

30. Pitcher MH, Cervero F (2010) Role of the NKCC1 co-transporter in sensitization of spinal nociceptive neurons. Pain 151: 756–762. doi: 10.1016/j.pain.2010.09.008 PMID: 20932645

31. Wei B, Kumada T, Furukawa T, Inoue K, Watanabe M, et al. (2013) Pre- and post-synaptic switches of GABA actions associated with Cl- homeostatic changes are induced in the spinal nucleus of the trigeminal nerve in a rat model of trigeminal neuropathic pain. Neuroscience 228: 334–348. doi: 10.1016/j.neuroscience.2012.10.043 PMID: 23103796

32. Nomura H, Sakai A, Nagano M, Umino M, Suzuki H (2006) Expression changes of cation chloride cotransporters in the rat spinal cord following intraplantar formalin. Neurosci Res 56: 435–440. doi: 10.1016/j.neures.2006.08.012 PMID: 17007947

33. Zhang W, Liu LY, Xu TL (2008) Reduced potassium-chloride co-transporter expression in spinal cord dorsal horn neurons contributes to inflammatory pain hypersensitivity in rats. Neuroscience 152: 502–510. doi: 10.1016/j.neuroscience.2007.12.037 PMID: 18262726

34. Galan A, Cervero F (2005) Painful stimuli induce in vivo phosphorylation and membrane mobilization of mouse spinal cord NKCC1 co-transporter. Neuroscience 133: 245–252. doi: 10.1016/j.neuroscience.2005.02.025 PMID: 15893647

35. Zhu Y, Lu SG, Gold MS (2012) Persistent inflammation increases GABA-induced depolarization of rat cutaneous dorsal root ganglion neurons in vitro. Neuroscience 220: 330–340. doi: 10.1016/j.neuroscience.2012.06.025 PMID: 22728089

36. Lin Q, Zou X, Willis WD (2000) Adelta and C primary afferents convey dorsal root reflexes after intradermal injection of capsaicin in rats. J Neurophysiol 84: 2695–2698. PMID: 11068011

37. Lee KY, Gold MS (2012) Inflammatory mediators potentiate high affinity GABA(A) currents in rat dorsal root ganglion neurons. Neurosci Lett 518: 128–132. doi: 10.1016/j.neulet.2012.04.068 PMID: 22580064

38. Prescott SA, De Koninck Y, Sejnowski TJ (2008) Biophysical basis for three distinct dynamical mechanisms of action potential initiation. PLoS ComputBiol 4: e1000198.

39. Zhu Y, Feng B, Schwartz ES, Gebhart GF, Prescott SA (2015) Novel method to assess axonal excitability using channelrhodopsin-based photoactivation. J Neurophysiol 113: 2242–2249. doi: 10.1152/jn.00982.2014 PMID: 25609112

40. Ratté S, Lankarany M, Rho YA, Patterson A, Prescott SA (2015) Subthreshold membrane currents confer distinct tuning properties that enable neurons to encode the integral or derivative of their input. Frontiers in cellular neuroscience 8: 452. doi: 10.3389/fncel.2014.00452 PMID: 25620913

41. Nusser Z (2009) Variability in the subcellular distribution of ion channels increases neuronal diversity. Trends Neurosci 32: 267–274. doi: 10.1016/j.tins.2009.01.003 PMID: 19299025

42. Zhu Y, Zhang XL, Gold MS (2014) Activity-dependent hyperpolarization of EGABA is absent in cutaneous DRG neurons from inflamed rats. Neuroscience 256: 1–9. doi: 10.1016/j.neuroscience.2013.10.004 PMID: 24135545

43. Prinz AA, Abbott LF, Marder E (2004) The dynamic clamp comes of age. Trends Neurosci 27: 218–224. doi: 10.1016/j.tins.2004.02.004 PMID: 15046881

44. Song Y, Li HM, Xie RG, Yue ZF, Song XJ, et al. (2012) Evoked bursting in injured Abeta dorsal root ganglion neurons: A mechanism underlying tactile allodynia. Pain 153: 657–665. doi: 10.1016/j.pain.2011.11.030 PMID: 22237000

45. Ratté S, Zhu Y, Lee KY, Prescott SA (2014) Criticality and degeneracy in injury-induced changes in primary afferent excitability and the implications for neuropathic pain. eLife 3: 02370.

46. Harper AA, Lawson SN (1985) Conduction velocity is related to morphological cell type in rat dorsal root ganglion neurones. JPhysiol (Lond) 359: 31–46.

47. Cho H, Yang YD, Lee J, Lee B, Kim T, et al. (2012) The calcium-activated chloride channel anoctamin 1 acts as a heat sensor in nociceptive neurons. Nat Neurosci 15: 1015–1021. doi: 10.1038/nn.3111 PMID: 22634729

48. Liu B, Linley JE, Du X, Zhang X, Ooi L, et al. (2010) The acute nociceptive signals induced by bradykinin in rat sensory neurons are mediated by inhibition of M-type K+ channels and activation of Ca2+-activated Cl- channels. J Clin Invest 120: 1240–1252. doi: 10.1172/JCI41084 PMID: 20335661

49. Takayama Y, Uta D, Furue H, Tominaga M (2015) Pain-enhancing mechanism through interaction between TRPV1 and anoctamin 1 in sensory neurons. Proc Natl Acad Sci U S A 112: 5213–5218. doi: 10.1073/pnas.1421507112 PMID: 25848051

50. Lee B, Cho H, Jung J, Yang YD, Yang DJ, et al. (2014) Anoctamin 1 contributes to inflammatory and nerve-injury induced hypersensitivity. Mol Pain 10: 5. doi: 10.1186/1744-8069-10-5 PMID: 24450308

51. Deba F, Bessac BF (2015) Anoctamin-1 Cl(-) channels in nociception: activation by an N-aroylaminothiazole and capsaicin and inhibition by T16A[inh]-A01. Mol Pain 11: 55. doi: 10.1186/s12990-015-0061-y PMID: 26364309

52. Jin X, Shah S, Du X, Zhang H, Gamper N (2016) Activation of Ca(2+) -activated Cl(-) channel ANO1 by localized Ca(2+) signals. J Physiol 594: 19–30. doi: 10.1113/jphysiol.2014.275107 PMID: 25398532

53. Segev I (1990) Computer study of presynaptic inhibition controlling the spread of action potentials into axonal terminals. JNeurophysiol 63: 987–998.

54. Cattaert D, El Manira A, Bevengut M (1999) Presynaptic inhibition and antidromic discharges in crayfish primary afferents. J Physiol Paris 93: 349–358. PMID: 10574123

55. Prescott SA, Sejnowski TJ, De Koninck Y (2006) Reduction of anion reversal potential subverts the inhibitory control of firing rate in spinal lamina I neurons: towards a biophysical basis for neuropathic pain. MolPain 2.

56. Verdier D, Lund JP, Kolta A (2003) GABAergic control of action potential propagation along axonal branches of mammalian sensory neurons. J Neurosci 23: 2002–2007. PMID: 12657657

57. Lian Y, Wang Y, Ma K, Zhao L, Zhang Z, et al. (2012) Expression of gamma-aminobutyric acid type A receptor alpha2 subunit in the dorsal root ganglion of rats with sciatic nerve injury. Neural regeneration research 7: 2492–2499. doi: 10.3969/j.issn.1673-5374.2012.32.002 PMID: 25337100

58. Fukuoka T, Tokunaga A, Kondo E, Miki K, Tachibana T, et al. (1998) Change in mRNAs for neuropeptides and the GABA(A) receptor in dorsal root ganglion neurons in a rat experimental neuropathic pain model. Pain 78: 13–26. PMID: 9822208

59. Monsivais P, Rubel EW (2001) Accommodation enhances depolarizing inhibition in central neurons. J Neurosci 21: 7823–7830. PMID: 11567073

60. Bal R, Oertel D (2001) Potassium Currents in Octopus Cells of the Mammalian Cochlear Nucleus. JNeurophysiol 86: 2299–2311.

61. Doyon N, Prescott SA, Castonguay A, Godin AG, Kroger H, et al. (2011) Efficacy of synaptic inhibition depends on multiple dynamically interacting mechanisms implicated in chloride homeostasis. PLoS Comput Biol 7: e1002149. doi: 10.1371/journal.pcbi.1002149 PMID: 21931544

62. Farrant M, Nusser Z (2005) Variations on an inhibitory theme: phasic and tonic activation of GABA(A) receptors. Nat Rev Neurosci 6: 215–229. doi: 10.1038/nrn1625 PMID: 15738957

63. Fischer Y, Parnas I (1996) Differential activation of two distinct mechanisms for presynaptic inhibition by a single inhibitory axon. J Neurophysiol 76: 3807–3816. PMID: 8985878

64. Lorenzo LE, Godin AG, Wang F, St-Louis M, Carbonetto S, et al. (2014) Gephyrin clusters are absent from small diameter primary afferent terminals despite the presence of GABA(A) receptors. J Neurosci 34: 8300–8317. doi: 10.1523/JNEUROSCI.0159-14.2014 PMID: 24920633

65. Tyagarajan SK, Fritschy JM (2014) Gephyrin: a master regulator of neuronal function? Nat Rev Neurosci 15: 141–156. doi: 10.1038/nrn3670 PMID: 24552784

66. Stell BM, Brickley SG, Tang CY, Farrant M, Mody I (2003) Neuroactive steroids reduce neuronal excitability by selectively enhancing tonic inhibition mediated by delta subunit-containing GABAA receptors. Proc Natl Acad Sci U S A 100: 14439–14444. doi: 10.1073/pnas.2435457100 PMID: 14623958

67. Essrich C, Lorez M, Benson JA, Fritschy JM, Luscher B (1998) Postsynaptic clustering of major GABAA receptor subtypes requires the gamma 2 subunit and gephyrin. Nat Neurosci 1: 563–571. doi: 10.1038/2798 PMID: 10196563

68. Brooks CM, Koizumi K (1956) Origin of the dorsal root reflex. J Neurophysiol 19: 60–74. PMID: 13286722

69. Dubuc R, Cabelguen JM, Rossignol S (1988) Rhythmic fluctuations of dorsal root potentials and antidromic discharges of primary afferents during fictive locomotion in the cat. J Neurophysiol 60: 2014–2036. PMID: 3236059

70. Desarmenien M, Santangelo F, Loeffler JP, Feltz P (1984) Comparative study of GABA-mediated depolarizations of lumbar A delta and C primary afferent neurones of the rat. Exp Brain Res 54: 521–528. PMID: 6327352

71. Wall PD (1959) Repetitive discharge of neurons. J Neurophysiol 22: 305–320. PMID: 13642103

72. Brooks CM, Koizumi K, Malcolm JL (1955) Effects of changes in temperature on reactions of spinal cord. J Neurophysiol 18: 205–216. PMID: 14368333

73. Rho YA, Prescott SA (2012) Identification of molecular pathologies sufficient to cause neuropathic excitability in primary somatosensory afferents using dynamical systems theory. PLoS Comput Biol 8: e1002524. doi: 10.1371/journal.pcbi.1002524 PMID: 22654655

74. Kim SH, Chung JM (1992) An experimental model for peripheral neuropathy produced by segmental spinal nerve ligation in the rat. Pain 50: 355–363. PMID: 1333581